A high-contrast coronagraph for the MMT using phase apodization: design and observations at 5 microns and 2 λ/D radius

J. L. Codona,* M. A. Kenworthy, P. M. Hinz, J. R. P. Angel, and N. J. Woolf

Steward Observatory, University of Arizona, Tucson, AZ 85721

We report on the first implementation of phase apodization for high-contrast imaging at close inner working angle. It is designed for use in the $5\,\mu\mathrm{m}$ M band with the adaptive optics system at the MMT, which uses a deformable secondary for low thermal background and achieves a Strehl ratio of 90% at $5\,\mu\mathrm{m}$. The method uses a diamond-turned ZnSe phase plate located at a cold pupil stop to diffract starlight into an "anti-halo" which suppresses the Airy diffraction pattern over a semi-circular region around the star. The design was optimized for strong suppression from the first bright Airy ring out to the control radius achievable with the MMT deformable secondary, about $9\lambda/D$. The time-averaged PSF of a bright star agrees well with the design profile, the core with FWHM of 0.18 arcsec showing the diffraction-limited resolution of the full aperture. At 0.34 arcsec radius ($2\lambda/D$) the floor level is 3.5×10^{-3} of the central peak, limited by residual atmospheric errors with 3 m wavelength across the aperture. The measured fluctuations at this radius averaged over 20 seconds are 2.5×10^{-4} rms (9 magnitudes down from the peak). With the addition of active feedback to control residual speckles caused by static wavefront errors and with longer exposures, we project that exoplanet searches should reach 5σ sensitivity level > 10 magnitudes in an hour of integration.

Keywords: Stellar Coronagraphs, Phase Masks, Phase Apodization, Extrasolar Planets.

1. INTRODUCTION

The search for faint companions, exoplanets, and diffuse structures such as dust disks around stars requires that the overwhelming starlight halo be suppressed. For even the nearest stars and the largest current generation telescopes, the interesting search area is confined to within a few λ/D of the star. Within this region, the unsuppressed stellar halo is much brighter than the expected companion objects, with the added problem of the residual adaptive optics (AO) speckle halo in ground-based telescopes. A popular approach has been to use a Lyot coronagraph with various improvements. Other methods have also been used and are reviewed by Guyon.[1]

Stellar coronagraphy on the ground has to contend with the additional problem of residual AO speckles and tip-tilt variations, which can move the star off the focal plane mask and allow a much brighter halo through. This problem can be addressed through fast tip-tilt compensation and more restrictive Lyot stops,[2] but it requires the additional complexity of a high-speed wavefront sensor and a servo control to keep the star centered on the mask. We are exploring the use of phase apodization in the pupil plane to suppress the diffraction pattern of the star. A special case of this has recently been studied by Yang and Kostinski.[3] Our approach has the same flavor, but is more general in the placement of the suppressed halo region and works for arbitrarily shaped pupils.

To make the most of the suppression, the residual AO speckle halo must be far below the star, which means that the potential is best in the mid-IR where the achievable AO Strehl ratio is high, but the sky background is still low enough not to be the detection constraint. We originally planned to use the MMT deformable secondary to create the pupil phase map, but creating a large enough phase gradient to achieve the diffraction suppression at, say, M-band would cause too great of a disruption to the PSF at the shorter wavelengths where the AO system's Shack-Hartmann wavefront sensor operates, causing the AO system to fail. We decided that since the diffraction pattern is primarily static, it could be suppressed using a static phase plate in a downstream pupil plane, allowing the fine tuning of the suppression to be addressed with the adaptive secondary with much smaller stroke requirements. For this first test, we used the Clio camera[4,5] on the MMT in the M-band, placing the phase plate in the Lyot stop filter wheel. This paper reports on the theory and design of the phase plate, and presents preliminary results from our first look at the PSF with Clio on the MMT.

*Author Info: jcodona@as.arizona.edu, http://caao.as.arizona.edu

Ground-based and Airborne Instrumentation for Astronomy, edited by Ian S. McLean, Masanori Iye,
Proc. of SPIE Vol. 6269, 62691N, (2006) · 0277-786X/06/$15 · doi: 10.1117/12.672727

2. THEORY

The phase plate was designed using the approach outlined as "Method I" in Codona & Angel, 2004.[6] We compute the required phase iteratively, with each iteration adding a small change to the overall phase. Each iteration takes some of the core starlight and diffracts it into an "antihalo" designed to suppress the remaining halo over a specified region of interest (ROI) in the focal plane. For this, we use a Fourier optics[7] treatment where the focal plane field ($\tilde{\psi}$) is given by the 2-D Fourier transform of the field in the pupil plane (ψ)

$$\tilde{\psi}(\boldsymbol{\kappa}) = \int d^2x\, e^{-i\boldsymbol{\kappa}\cdot\boldsymbol{x}} \Pi(\boldsymbol{x})\psi(\boldsymbol{x}), \tag{1}$$

where $\boldsymbol{x}$ is the position in the pupil plane, $\Pi(\boldsymbol{x})$ is the pupil mask, $\boldsymbol{\kappa}$ is the 2-D spatial frequency corresponding to the angular position in the focal plane relative to the star as $\boldsymbol{\theta} = \boldsymbol{\kappa}/k$, and $k = 2\pi/\lambda$. The original diffraction halo ($\tilde{\psi}_0(\boldsymbol{\kappa})$) is given by eq. (1) with the incoming field equal to a unit plane wave, or $\psi_0 = 1$. If the pupil function is purely real, the resulting halo has Hermitian symmetry, $\tilde{\psi}_0(-\boldsymbol{\kappa}) = \tilde{\psi}_0^*(\boldsymbol{\kappa})$. Introducing a small phase aberration $\varphi(\boldsymbol{x})$ ($\varphi \in \mathbb{R}$ and $|\varphi| \ll 1$) in the pupil plane results in the modified halo

$$\begin{aligned} \tilde{\psi}(\boldsymbol{\kappa}) &= \int d^2x\, e^{-i\boldsymbol{\kappa}\cdot\boldsymbol{x}} e^{i\varphi(\boldsymbol{x})} \Pi(\boldsymbol{x})\psi_0(\boldsymbol{x}) &(2)\\ &\approx \tilde{\psi}_0(\boldsymbol{\kappa}) + i\int d^2x\, e^{-i\boldsymbol{\kappa}\cdot\boldsymbol{x}} \varphi(\boldsymbol{x})\Pi(\boldsymbol{x})\psi_0(\boldsymbol{x}). &(3)\end{aligned}$$

The extra term in eq. (3) is the piece we are going to manipulate into suppressing the diffraction halo. We call it the "antihalo" term. Since the phase is real, but is multiplied by i, the antihalo term is anti-Hermitian. This difference in symmetry between the diffraction halo and the kinds of antihalo structures we can form using phase shifts, means that we cannot simultaneously suppress the halo on both sides of the star. We can, however, suppress an arbitrary halo over some region of the focal plane, just not on opposite sides of the star. Selecting this ROI, along with the specified pupil, determines the phase required to suppress the halo.

In order to suppress the halo over the ROI, we use eq. (3) to compute the best additional phase which suppresses the halo over the ROI, and add it to the last estimate of the best phase, compute the new halo and repeat. At each point in the calculation, the new halo is still non-zero, but can be further reduced by the same method. The additional phase adds up to a value which is large compared with unity (typically larger than 2π), but since the individual steps are small, the linear Taylor expansion in eq. (3) is still valid.

We proceed by using eq. (3) from the nth to the $(n+1)$st iteration:

$$\tilde{\psi}_{n+1}(\boldsymbol{\kappa}) = \tilde{\psi}_n(\boldsymbol{\kappa}) + i\int d^2x\, e^{-i\boldsymbol{\kappa}\cdot\boldsymbol{x}} \varphi_n(\boldsymbol{x}) e^{i\phi_n(\boldsymbol{x})} \Pi(\boldsymbol{x}), \tag{4}$$

where $\phi_n(\boldsymbol{x}) = \sum_{m=1}^{n-1} \varphi_m(\boldsymbol{x})$ and $\phi_{n+1} = \varphi_n + \phi_n$. Since our goal is to make $\tilde{\psi}_{n+1}(\boldsymbol{\kappa}) = 0$ over the ROI, we assume that we are successful and solve for the required phase. Thus, for $\boldsymbol{\kappa} \in ROI$,

$$i\tilde{\psi}_n(\boldsymbol{\kappa}) = \int d^2x\, e^{-i\boldsymbol{\kappa}\cdot\boldsymbol{x}} \varphi_n(\boldsymbol{x}) e^{i\phi_n(\boldsymbol{x})} \Pi(\boldsymbol{x}). \tag{5}$$

If we had information for the entire focal plane, rather than just the ROI, we could solve for the required phase with an inverse Fourier transform. This is not possible however, so we do what we can by masking off the ROI and inverse Fourier transforming what we do have. The result is

$$\frac{i}{(2\pi)^2}\int_{ROI} d^2\kappa\, e^{i\boldsymbol{\kappa}\cdot\boldsymbol{x}} \tilde{\psi}_n(\boldsymbol{\kappa}) = \int d^2x'\, \varphi_n(\boldsymbol{x}') e^{i\phi_n(\boldsymbol{x}')} \Pi(\boldsymbol{x}')\mathcal{H}(\boldsymbol{x}-\boldsymbol{x}'), \tag{6}$$

where $\mathcal{H}(\boldsymbol{x}) = \int_{ROI} d^2\kappa\, \exp(i\boldsymbol{\kappa}\cdot\boldsymbol{x})$ is the spatial filter corresponding to the region of interest. Since the ROI does not include the entire focal plane, $\mathcal{H}(\boldsymbol{x}) \neq \delta(\boldsymbol{x})$. However, if the ROI is reasonably large in terms of λ/D scales, $\mathcal{H}(\boldsymbol{x})$ is fairly compact. For this initial version of the phase mask, we made the relatively crude approximation that the spatial filter is indeed a delta function times a constant, $\mathcal{H}(\boldsymbol{x}) \to h\delta(\boldsymbol{x})$. One of the consequences of this approximation is the inability

to suppress all of the fine structure of the halo in the focal plane. This can all be properly handled, but it adds unnecessary complexity to the present solution when the only place it will matter is hidden under the residual AO speckle halo. So we make the substitution for $\mathcal{H}(\boldsymbol{x}-\boldsymbol{x}')$ and find

$$h\varphi_n(\boldsymbol{x})e^{i\phi_n(\boldsymbol{x})}\Pi(\boldsymbol{x}) = \frac{i}{(2\pi)^2}\int_{ROI} d^2\kappa\, e^{i\boldsymbol{\kappa}\cdot\boldsymbol{x}}\tilde{\psi}_n(\boldsymbol{\kappa}). \tag{7}$$

Now, using $\tilde{\psi}_n(\boldsymbol{\kappa}) = \int d^2x\, e^{-i\boldsymbol{\kappa}\cdot\boldsymbol{x}}e^{i\phi_n(\boldsymbol{x})}\Pi(\boldsymbol{x})$, changing the order of integration, and taking the real part since the phase must be real (n.b. $\Re(iz) = -\Im(z)$ for complex z), we can solve for the new increment in phase. Adding this new increment to the last estimate, we find the new phase estimate is

$$\phi_{n+1}(\boldsymbol{x}) = \phi_n(\boldsymbol{x}) - \Im\left\{e^{-i\phi_n(\boldsymbol{x})}\int d^2x'\, e^{i\phi_n(\boldsymbol{x}')}\Pi(\boldsymbol{x}')\mathcal{H}(\boldsymbol{x}-\boldsymbol{x}')/h\right\}. \tag{8}$$

Although the constant h is determined by integrating a testing function against $\mathcal{H}(\boldsymbol{x}-\boldsymbol{x}')$, it can be treated as a free parameter and adjusted to aid in convergence.

This algorithm is good enough for testing purposes and quite probably good enough for generating practical phase plates for initial scientific surveys in the mid-IR. However, it suffers from two shortcomings. The first is that by approximating the spatial filter term with a delta function, we are mis-matching the larger spacing phase correlations with the required antihalo at each step. Thus, fine structure background or rapid variations in the PSF will not be well matched by the antihalo and and will ultimately limit the depth of our suppression. As is shown below, this is not likely to be an immediate performance limitation in ground-based astronomical applications since the residual AO speckle halo is still fairly bright and will limit detections. However, a more careful mathematical treatment *will* be important for space-based applications where the contrast with the background can be much greater. In general, it is much more important to maximize the Strehl ratio of the phase plate. This brings us to the second shortcoming of this treatment: Strehl ratio. Unlike the classic Slepian derivation leading to the rectangular[8] and circular prolate spheroidal[9] transmission apodizations, which minimize the power in the halo while simultaneously maximizing the power in the core, we have only minimized the power in the halo over the ROI. The fact that we performed our calculation directly on the field rather than by applying a calculus of variations on integrals of the PSF intensity is not a critical difference. Rather, it is our neglect of the core that can be a problem. Therefore, it is generally true that our Strehl is lower than it could be. The theory for the full problem, treating both the fine structure halo residual and optimally preserving the Strehl ratio of the phase plate has recently been worked out and will be presented in an upcoming paper.

Background contrast and deciding where to stop

Iterating eq. (8) yields a halo which is reasonably dark within the ROI, but at a cost in Strehl ratio. The Strehl ratio of the phase plate is given by

$$\mathcal{S}_\phi = \left|\frac{\int e^{i\phi(\boldsymbol{x})}\Pi(\boldsymbol{x})\, d^2x}{\int \Pi(\boldsymbol{x})\, d^2x}\right|^2. \tag{9}$$

The Strehl ratio of the telescope's AO system ($\mathcal{S}_{AO}$) is taken from the inbound starlight first, with $(1-\mathcal{S}_{AO})$ of the light going into the residual speckle halo. The speckle halo is rapidly changing and essentially unaffected by the downstream phase plate. As such, the averaged speckle halo acts much like any other incoherent background, such as sky noise. The only important difference is that the speckle background is proportional to the star's flux. For this discussion we will assume that the speckle halo is the next most dominant source of photon noise as the diffraction halo is suppressed. The Strehl ratio of the phase plate further drops the PSF of the star, as well as any surrounding objects, into the speckle noise as the halo in the ROI is suppressed. This means that as the diffraction halo is further suppressed, the S/N will eventually become limited by the speckle halo or other background, and further halo suppression will actually make the detection sensitivity worse. Possibly accelerating this phenomenon is the fact that eq. (8) does not specifically include the preservation of the PSF core as it suppresses the halo. To avoid going too far, we watch the Strehl ratio of the phase mask and the suppressed halo contrast in the ROI as the algorithm proceeds and stop it when the improved detection S/N is maximized.

We do this by monitoring an SNR metric, derived as follows. Imagine an exoplanet with a contrast of p from the star. The "signal" from this exoplanet is

$$\text{Signal} = p\Phi_{star}\mathcal{S}_{AO}\mathcal{S}_\phi,$$

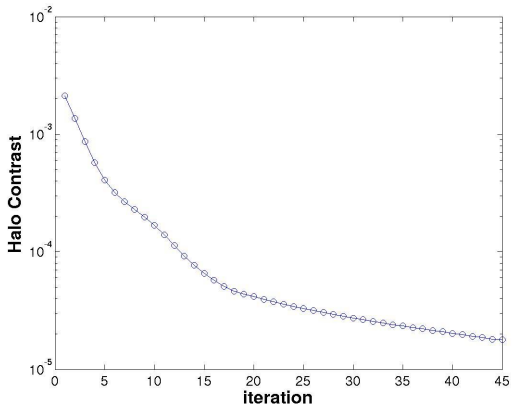

(a) A representative halo contrast value plotted against iteration number.

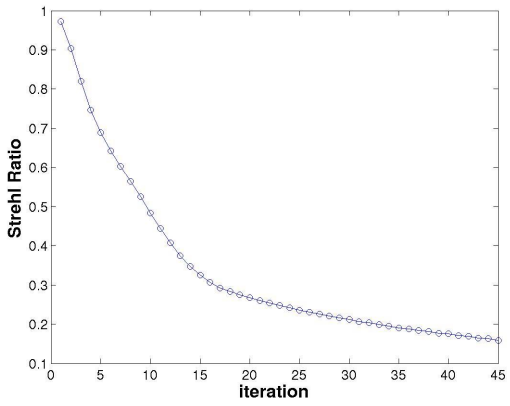

(b) Phase plate Strehl ratio history vs. iteration number.

Figure 1. The histories of a representative halo contrast and the phase plate Strehl ratio over the course of the iteration.

where Φ_{star} is the star's photon flux. The "noise" against which this detection is made is the combination of the residual AO speckle halo (with initial contrast C_{AO}) and the remaining diffraction halo (which has different contrast to the peak for each stage of the calculation), which is therefore a function of the phase plate Strehl ratio, $C_{halo}(\mathcal{S}_\phi)$, measured relative to the fading peak of the star's PSF. Even though these two backgrounds both derive from the starlight and are instantaneously coherent, the rapid variation of the speckle halo makes them incoherent in the average. The background noise over the same patch as the exoplanet is given by

$$\text{Background Noise} = (C_{AO} + \mathcal{S}_\phi C_{halo}(\mathcal{S}_\phi))\Phi_{star}\mathcal{S}_{AO}.$$

The detection of the exoplanet is made against the standard deviation of the background noise. Thus the S/N is proportional to

$$S/N \propto \frac{\mathcal{S}_\phi}{\sqrt{C_{AO} + \mathcal{S}_\phi C_{halo}(\mathcal{S}_\phi)}}. \tag{10}$$

At each step of the iteration we compute $\mathcal{S}_\phi$, as well as make an estimate of the halo contrast in the ROI. We have estimated the M-band Strehl ratio at the MMT to exceed 90% with a speckle halo contrast of around 3 decades. Figure 1 shows the calculation's Strehl ratio and halo suppression histories, and figure 2 shows the corresponding SNR metric values from eq. (10) plotted against iteration number and phase plate Strehl ratio. Note that, as usual, if the core-to-speckle halo contrast is poor (i.e. low Strehl ratio), there is no use in using a coronagraphic phase plate. As the AO Strehl ratio rises and the speckle halo drops relative to the star, the value of using the plate becomes more pronounced. Pushing the halo dark zone lower than the background actually hurts the detection sensitivity. This determines the stopping criterion for the calculation.

Effect of detector bandwidth

Suppressing diffraction by introducing aberrations is inevitably chromatic. The practical effect is that the dark zone in the halo begins to brighten with increasing bandwidth. However, so long as the combined halo remains sufficiently below the residual AO speckle halo, it won't significantly limit detection. However, in practice, the advantage of using phase apodized pupils with larger bandwidths is greater than might at first be supposed. Codona & Angel[6] pointed out that the amplitude deviation between the diffraction halo and the constructed antihalo grows linearly with $|\lambda - \lambda_0|$ where λ_0 is the wavelength where the eq. 8 iteration was performed. This leads to a brightening of the suppressed narrowband halo proportional to $(\lambda - \lambda_0)^2$ and a full-band brightening proportional to the cube of the detector bandwidth. This implies a fairly narrow usable bandwidth of only a few percent. However, this is only strictly true in the case where the suppression

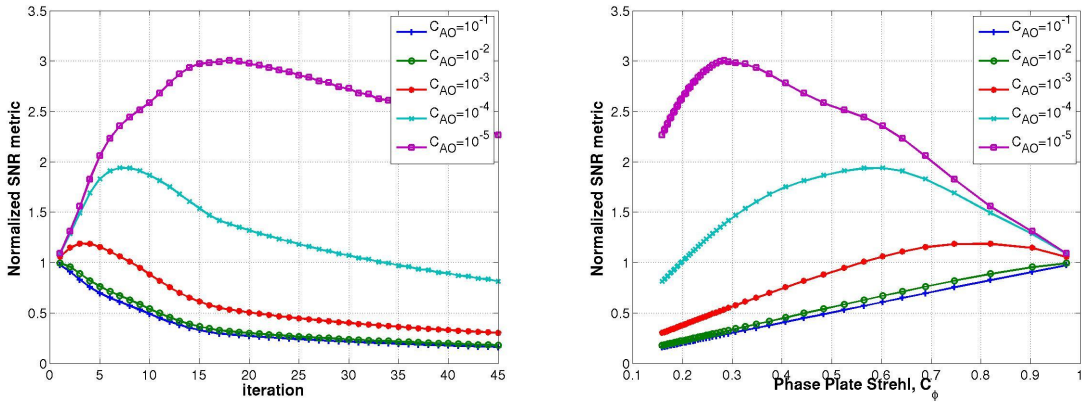

(a) SNR metric plotted against iteration number.

(b) SNR metric plotted against the Strehl ratio of the phase plate.

Figure 2. SNR Metric versus iteration and $\mathcal{S}_\phi$ for various AO Strehl ratios (i.e. initial AO halo contrasts). As expected, the potential sensitivity improvement increases with better AO system performance. Depending on the wind, the MMT M-band AO 90% Strehl contrast between the PSF peak and the speckle halo is expected to lie between about 2×10^{-3} and 10^{-4} between 2 and 10 λ/D.

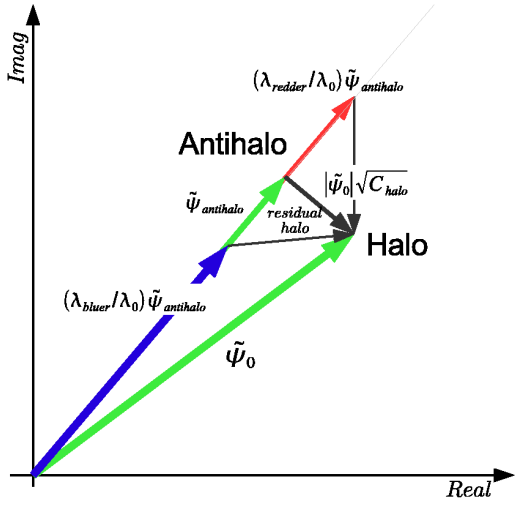

Figure 3. Complex halo geometry showing the effect of wavelength. The intensity of the original halo is reduced by subtracting the antihalo phasor. In κ-space, the diffraction halo doesn't change its position with wavelength, and since the height map of the phase plate is independent of λ, the phase of an antispeckle relative to the core will not change either. However, since the phase is implemented by a geometric surface, the antihalo amplitude scales with λ. This scales the antihalo phasor without wrapping it, and the typical best distance means that there is a softer takeoff for the halo brightening than if it were perfectly matched.

has perfectly suppressed the halo. There the wavelength-dependent brightening quickly grows to overwhelm the very dark suppressed halo. What we saw in the last section was that if we are otherwise background limited in our detection, we are better off not making the halo too dark, since it overly harms the signal we are trying to detect. Therefore, the complex halo and antihalo are not perfectly matched, but have a residual error amplitude of the order of $\sqrt{C_{halo}}\tilde{\psi}_0$. At a given $\boldsymbol{\kappa}$ in the ROI, $\tilde{\psi}_0(\boldsymbol{\kappa})$ is independent of wavelength, while the antihalo diffracted by the Fourier component of the phase shifts across the phase plate maintains its complex phase (since the physical position of the phase plate structure doesn't change), while the amplitude is proportional to the wavelength. Since there is a halo-antihalo mismatch at λ_0, the typical incorrect

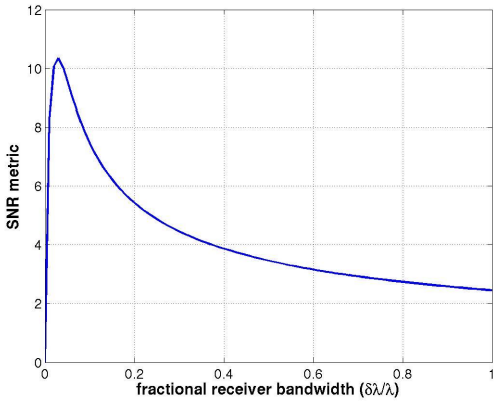

Figure 4. SNR metric plotted against fractional receiver bandwidth. The sensitivity peaks at a narrow bandwidth, but then falls off slowly as $B^{-1/2}$. Best performance is achieved at the peak, given by eq. (12).

antihalo will continue to miss the halo for all wavelengths in the vicinity of λ_0 . For ease of estimation, we will treat the best halo contrast as determining an "impact parameter" for the halo-antihalo distance (figure 3). From this argument and treating the spectra of the star and the exoplanet as reasonably flat, we find that eq. (10) becomes

$$S/N \propto \frac{\mathcal{S}_\phi \sqrt{B}}{\sqrt{C_{AO} + \mathcal{S}_\phi (C_{halo} + B^2/12)}}, \tag{11}$$

where B is the fractional receiver bandwidth. That is, $\lambda_0(1 - B/2) < \lambda < \lambda_0(1 + B/2)$. Since there are fewer photons available in a narrower band, the S/N is worse for very narrow bands, while beyond an optimum bandwidth, the brightening halo begins to dominate detection sensitivity. The optimum bandwidth is given by

$$B_{best} = \sqrt{12(C_{AO}/\mathcal{S}_\phi + C_{halo})}. \tag{12}$$

While this bandwidth is the best, larger bandwidths only hurt the S/N as $B^{-1/2}$, which is slow enough that using even larger bandwidths may still be of use, even though the sensitivity will be somewhat reduced.

3. CLIO PHASE PLATE DESIGN

We made a real phase plate to validate the design principles and methodology. We used the Clio camera which allowed us to place the phase plate into a filter wheel in a reimaged pupil plane (Lyot plane). Clio is designed to operate in the mid-IR, where the MMT AO system has achieved Strehl ratios of 90%. As shown above, the efficacy of the phase plate method is better with higher Strehls. We originally intended to do testing with the Clio camera on either the Steward Observatory 61" Kuiper telescope or the MMT, which meant that the details of the pupil would be different. Although the phase plate design algorithm is able to handle arbitrary pupils, including secondary obstructions and spider supports, etc., we wanted to be independent of these differences for testing. We also wanted to avoid the operational complexity of precisely aligning a phase plate with the reimaged pupil, and rotating the mask azimuthally to exactly match the orientation of the spider vanes. To avoid these problems, we decided to separately make a *known* pupil mask with an undersized outer "primary" diameter and and an oversized "secondary" obstruction. We also used a conservatively oversized spider vane support which would hide the real spider even with a few degree rotation error of the mask (fig 5a). We had the plate manufactured by *II-VI Infrared* by diamond-turning ZnSe which has an index of refraction $n = 2.43$ at $\lambda = 4.68\mu m$. The iterative algorithm generates a phase map for the plate, which was mapped into a physical surface displacement of the ZnSe using the formula $z = \phi\lambda/2\pi(n-1)$. To fit the Clio camera pupil filter wheel, we needed a piece with 1/2 inch diameter and a 4.47 mm radius active area. The phase plate was manufactured with fiducial marks indicating the center of the mask and the orientation of the spider vanes. The fiducial marks were designed to be hidden under the mask "secondary" or outside of the active area entirely.

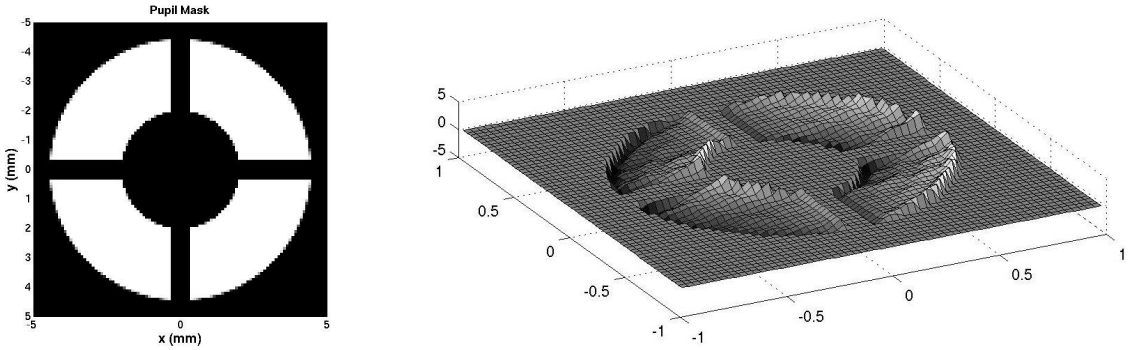

(a) Pupil mask used in the phase mask calculation.

(b) The phase map used in the Clio MMT experiment.

Figure 5. The pupil mask and resulting phase map for the Clio MMT test.

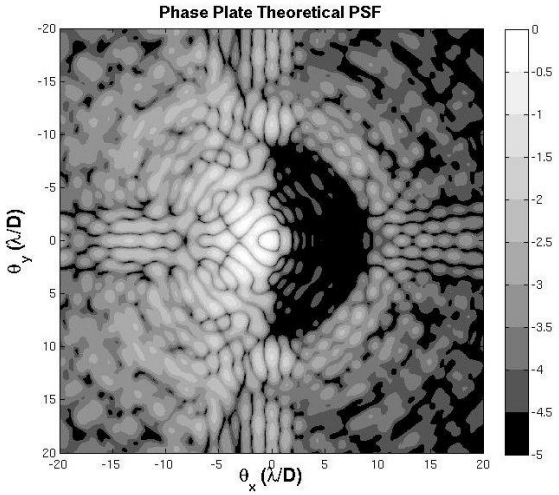

Figure 6. The computed PSF for the phase plate, for a 5% band centered on $4.67\mu\mathrm{m}$.

The MMT adaptive secondary has 336 actuators, which corresponds to a control radius of approximately $9\lambda/D$. We chose a region of interest which included the maximum of 180° in position angle, running from 2 to $10\lambda/D$ from the star, where D is in mask diameters as projected back to the full-scale pupil plane. The edges of the ROI were all smoothly anti-aliased by using a smooth masking function. The result was that over the filter band the dark zone extended out roughly to the control radius of the AO system, and suppressing somewhat into the first Airy ring. The radial spreading of the halo with bandwidth brings the effective outer working radius in to $\sim 9\lambda/D$.

Since lag errors causes a peaking of the speckle halo toward the center of the PSF, depending on the wind and the temporal evolution of the atmospheric turbulence, a Strehl ratio of 90% corresponds to a speckle halo contrast of about 2×10^{-3} and 10^{-4} between 2 and $10\lambda/D$. According to figure 2, this would indicate stopping with a plate Strehl ratio of 0.6 to 0.8. However, since the first phase plate was to be used for engineering studies and looking at bright stars, we decided to be very conservative and push the diffraction halo farther below the expected AO speckle halo than indicated to ensure that we could make an uncontaminated estimate of the residual AO speckle halo. We ended up with a phase plate with a Strehl ratio $\mathcal{S}_\phi \approx 29\%$. This choice achieved its engineering goal, but was likely a marginal choice in terms of sensitivity improvement. The next generation of phase plate will be designed with a higher Strehl and less aggressive halo suppression.

4. MMT RESULTS

Once the prototype phosphor-bronze mask and phase plate were manufactured, they were manually aligned and held in place with adjustable clips (figure 7). The assembled unit was inserted into the Clio camera at the intermediate pupil plane and mechanically positioned into the telescope beam using a motorized filter wheel. Clio has a pupil imaging mode which allowed quick and easy alignment of the phase plate assembly with the telescope pupil. To go from direct imaging to phase plate imaging typically took on the order of five minutes.

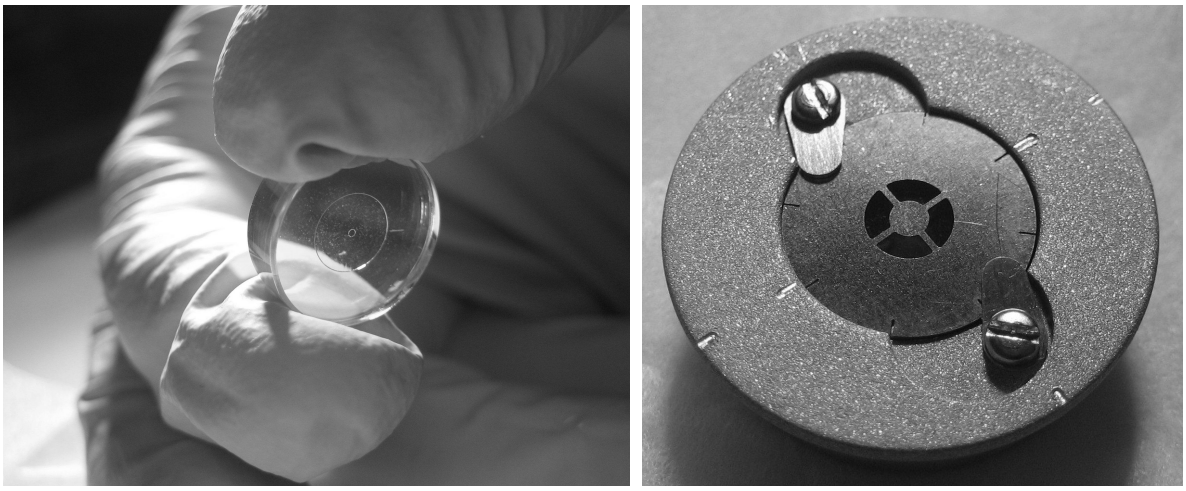

(a) ZnSe diamond-turned phase plate. Note fiducial marks.

(b) Completed assembly of phase plate and pupil mask.

Figure 7. The completed phase plate and pupil mask assembly.

Clio is an imager designed for obtaining high spatial resolution images with optimum efficiency at L' and M band. It is optimized for imaging extrasolar planets, where the planets are expected to have flux significantly in excess of that of a similar temperature blackbody.[10,11] Clio's plate scale in the M-band is about $0.3\lambda/D$ per pixel. We observed Vega on two nights using the phase plate at the $f/15$ Cassegrain focus of the MMT 6.5m telescope, with the AO system operating in closed loop on the target star. Images were taken using a narrowband filter in M ($\lambda_c = 4.67\mu m$, $\lambda_{fwhm} = 0.25\mu m$). We estimated the Strehl ratio of the AO system to be greater than 90% at M band, resulting in 10% of the incoming light being distributed in a speckle halo of similar size to the seeing disk at this wavelength. The data were taken on a night where the mean uncorrected seeing was 0.8 arcseconds at R band.

Figure 8 shows images of Vega before and after inserting the phase plate. The structure of the PSF is remarkably consistent with the calculations, as shown in figure 6. In significant contrast with transmission apodization methods or with Lyot coronagraphs with sufficiently undersized Lyot stops, the PSF core retains a FWHM of 0.18 arcsec, showing the diffraction-limited resolution of the full aperture. At 0.34 arcsec radius ($2\lambda/D$) the floor level is 3.5×10^{-3} of the central peak, where it is limited by the residual AO errors with scales of approximately 3 m across the aperture. We estimated the fluctuations at this radius, averaged over 20 seconds, to be $\sim 2.5 \times 10^{-4}$ rms (i.e. 9 magnitudes down from the peak). Detailed examination of the images show faint static residual speckles which likely result from slight irregularities in the phase plate's manufacturing, or, more likely, by mismatches and misalignments between the pupil mask and the phase plate. Such errors can be compensated for using biases applied to the MMT's adaptive secondary.[12] With the addition of this active feedback to control residual speckles caused by static wavefront errors and longer exposures, we project that exoplanet searches should reach 5σ sensitivity level > 10 magnitudes in an hour of integration.

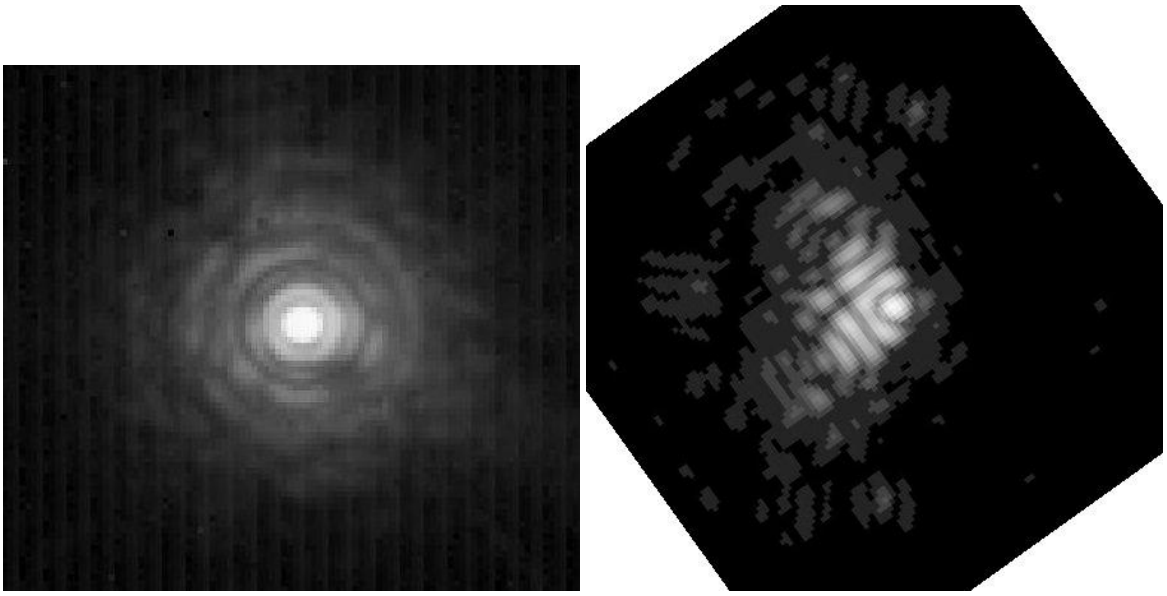

(a) Image without the phase plate.

(b) Image taken with the phase plate.

Figure 8. The coadded images of Vega taken using Clio without (a) and with (b) the phase plate.

5. CONCLUSIONS

Phase apodization appears to work in accordance with theory, opening up a potentially fruitful new technique for examining the regions very near stars. One of the great advantages of the method is ease of use, in that it does not require carefully placing the star on a focal plane mask. Rather, it permits a coronagraphic capability to be included in a filter wheel set, to be used as needed with no other special provisions. The performance limitation is ultimately set by the contrast ratio between the star and the background. In this paper we assumed that the background was due to the residual AO speckle halo, which was the case with the Vega observations. However, the fainter stars that would be in a survey would likely be limited by sky noise. In that case, the analysis indicates that a less aggressive halo suppression is best. This tradeoff is further optimized by maintaining the highest possible phase plate Strehl ratio for a given level of halo suppression. The mathematical approach used here did not specifically preserve the PSF core, but simply suppressed the halo at all costs. An improved and more complete theory has now been developed, allowing both darker halos and optimally maintained Strehl ratios. This new method will be used for designing future phase plates. The phase plate, and indeed any real optic, will have residual imperfections which cause deviations from ideal performance. By having used the phase plate to achieve most of the halo suppression, the remaining stroke requirements are sufficiently small that biases applied to the adaptive secondary can be used to suppress the remaining error speckles without harming the operation of the AO closed loop. This means that we can achieve an actively maintained optimal coronagraphic capability, while retaining the low surface count and low emissivity of the MMT.

6. ACKNOWLEDGMENTS

This work was supported by NASA through the NASA Astrobiology Institute, under Cooperative Agreement No. CAN-02-OSS-02 #NNA04CC07A, issued through the Office of Space Science. The mathematical theory was developed in part under grants from NASA, APRA04-0013-0056, and the NSF, AST-0138347.

REFERENCES

1. Guyon, O. “Limits of Adaptive Optics for High-Contrast Imaging”, ApJ, **629,** 592-614, 2005.

2. Codona, J. L. “Stellar coronagraphs for telescopes with arbitrary pupils”, in *Astronomical Adaptive Optics Systems and Applications*, eds. R. K. Tyson & M. Lloyd-Hart, Proc. SPIE **5169**, 228-237, San Diego, CA, 2003.
3. Yang W. and Kostinski, A. B., “One-sided Achromatic Phase Apodization for Imaging of Extrasolar Planets”, ApJ, **605**, 892-901, 2004.
4. Freed, M., Hinz, P. M., Meyer, M. R., Milton, N. M., and Lloyd-Hart, M., “Clio: A 5 micron camera for the detection of giant exoplanets”, in *Ground-based Instrumentation for Astronomy*, eds. A. Moorwood & M. Iye, **5492**, 1561-1571, Glasgow, Scotland, U.K., 2004.
5. Sivanandam, S., Hinz, P. M., Heinze, A.N., & Freed, M. “Clio: a 3-5 micron AO planet-finding camera, status report”, in *Ground-based and Airborne Instrumentation for Astronomy*, Proc. SPIE, **6269**, Orlando, FL, 2006.
6. Codona, J. L. and Angel, R. “Imaging extrasolar planets by stellar halo suppression in separately-corrected color bands”, ApJ, **604** , L117-L120, 2004.
7. Goodman, J. W., *“Introduction to Fourier Optics"*, McGraw-Hill, New York, NY, 1995.
8. Slepian, D., and H. O. Pollack, “Prolate spheroidal wave functions, fourier analysis and uncertainty”, Bell System Tech. J.**, 40**, 43-84, 1961.
9. Slepian, D., “Analytic solution of two apodization problems”, JOSA, **55**(9), 1110-1115, 1965.
10. Baraffe, I., Chabrier, G., Barman, T. S., Allard, F., & Hauschildt, P. H. “Evolutionary models for cool brown dwarfs and extrasolar giant planets. The case of HD 209458”, A&A, **402**, 701-712, 2003.
11. Burrows, A., Sudarsky, D., & Lunine, J. I. “Beyond the T Dwarfs: Theoretical Spectra, Colors, and Detectability of the Coolest Brown Dwarfs”, ApJ, **596**, 587-596, 2003.
12. Kenworthy, M. A., Hinz, P. M., Angel, J. R. P., Heinze, A. N., Sivanandam, S., “Whack-a-speckle: focal plane wavefront sensing in theory and practice with a deformable secondary mirror and 5-micron camera”, in *Advances in Adaptive Optics II*, eds. B. L. Ellerbroek & D. B. Calia, Proc. SPIE, **6272**, Orlando, FL, 2006.